2019 American Control Conference (ACC)
Philadelphia, PA, USA, July 10-12, 2019

Hybrid System Model of Microextrusion-Based Direct-Write Additive Manufacturing

Ali Asghari Adib and David Hoelzle

Abstract— **Flowrate control in Direct-Write (DW) Additive Manufacturing (AM) continues to be a challenge due to a capacitative energy storage in the system and the absence of suitable flowrate sensors at the micro-scale. Lack of precise control leads to an excess or a lack of ink while printing, resulting in manufacturing defects. The incorporation of a pressure sensor and a feedback controller is a potential approach for precisely controlling the flowrate. However, in the case where the ink loses contact with the pressure sensor, there will be an abrupt loss in feedback signal, which could potentially result in instability in the closed loop. In this paper, we present a hybrid model that represents the continuous dynamics of microextrusion with discrete switching between three different modes that captures the presence or loss of a sensed pressure. The simulation results demonstrate that the model captures the continuous dynamics of microextrusion while switching between three discrete modes: normal printing mode, retracted ink leading edge mode, and loss of pressure signal mode. The hybrid model presented here paves the way for switched controller synthesis to create stable feedback controllers.**

I. INTRODUCTION

Developments in the field of additive manufacturing (AM) have enabled the layer by layer fabrication of complex 3D structures from computer models [1]. One class of AM tools, direct-write (DW) AM, has demonstrated success in printing a wide range of ink formulations, in millimeters to nanometers scale [1], for various industrial [2], and biomedical applications [3], [4], [5], [6]. In extrusion based DW printing, such as Micro Robotic Deposition (μRD) [3], [7], the ink, or the material, is pneumatically or mechanically extruded from a nozzle that can move in *xyz* axes enabling 3D deposition on the substrate.

Ink characteristics and flow dynamics are key factors in successful DW printing. However, despite the body of literature on dynamic modeling and control of inks in DW AM [3], [8], [9], precise control of flowrate is still a challenge introducing defects in printed structures. For instance, system compliances in DW printing result in a lack of ink when starting ink flowrate and an excess of ink when stopping ink flowrate [10]. Previously, we developed an iterative learning control (ILC) based method to control the flowrate in microextrusion [10]. However, despite the effectiveness of the developed method, ILC based methods learn the correct flowrate signal for a single ink and extruder configuration and have to be retrained for any deviation from the learned behavior, increasing the production time and consuming of the ink.

Ideally, flowrate is controlled with simple feedback controllers. Although there is an absence of suitable flowrate sensors at DW AM scale, there are well-established relationship between flowrate and pressure through a fluidic resistance ($Q = f(P)$ where Q is the flowrate and P is pressure [11]) that motivates the incorporation of pressure sensors into the system. Pressure sensors are inexpensive and easily integrated at the microscale. Therefore, in principle, accurate flowrate control in DW AM using microextrusion can be achieved by incorporating a pressure sensor and a feedback controller into the normal DW system. However, this system configuration introduces a new problem. Consider the sequence of events diagrammed in Fig. 1. At time $t = t_1$, ink is being extruded through the nozzle and is in contact with a pressure sensor, thus the pressure sensor reads the pressure in the fluid (Mode 1). At $t = t_2$, ink has stopped extruding; the ink leading edge is at position a (Mode 2). At $t = t_3$, the ink has receded so far that the ink is no longer in contact with the pressure sensor; the sensor is now reading the ambient pressure in the air and has no information on the ink pressure (Mode 3). If the syringe piston displaces again in the positive direction, the ink leading edge will contact the sensor again, ($t = t_4$), and sensor will again read the fluid pressure (Mode 2 again). With the loss of feedback signal in Mode 3, certain controller designs, particularly those using integrators, will not be stable.

Hybrid system modeling can be employed to describe the dynamics of a system having both continuous and discrete states. Hybrid system modeling and control has been successfully used in many different applications such as air traffic control [12], automotive control [13], switching power converters [14], and robotics [15], [16]. This paper presents a hybrid system model to formulate the dynamics of microextrusion with pressure feedback for future control synthesis and analysis. The microextrusion process have both continuous and discrete dynamics, which has been addressed for other types of AM systems, [17], but never before for extrusion-based DW. Section II presents the model assumptions and the continuous and discrete dynamics, including the switching criteria for switching between different discrete modes. Section III provides the details of a simulation study that cycles the system through the three system modes. Section IV, provides the flowrate, pressure, and ink leading edge responses and then Section V discusses important aspects of the study and proposed future research directions.

*This work was supported by NSF CMMI-1708819

A. Asghari Adib is with the Department of Mechanical Engineering, Ohio State University, Columbus, OH 43210, USA asghariadib.1 at osu.edu

D. Hoelzle is with the Department of Mechanical Engineering, Ohio State University, Columbus, OH 43210, USA hoelzle.1 at osu.edu

978-1-5386-7926-5/$31.00 ©2019 AACC

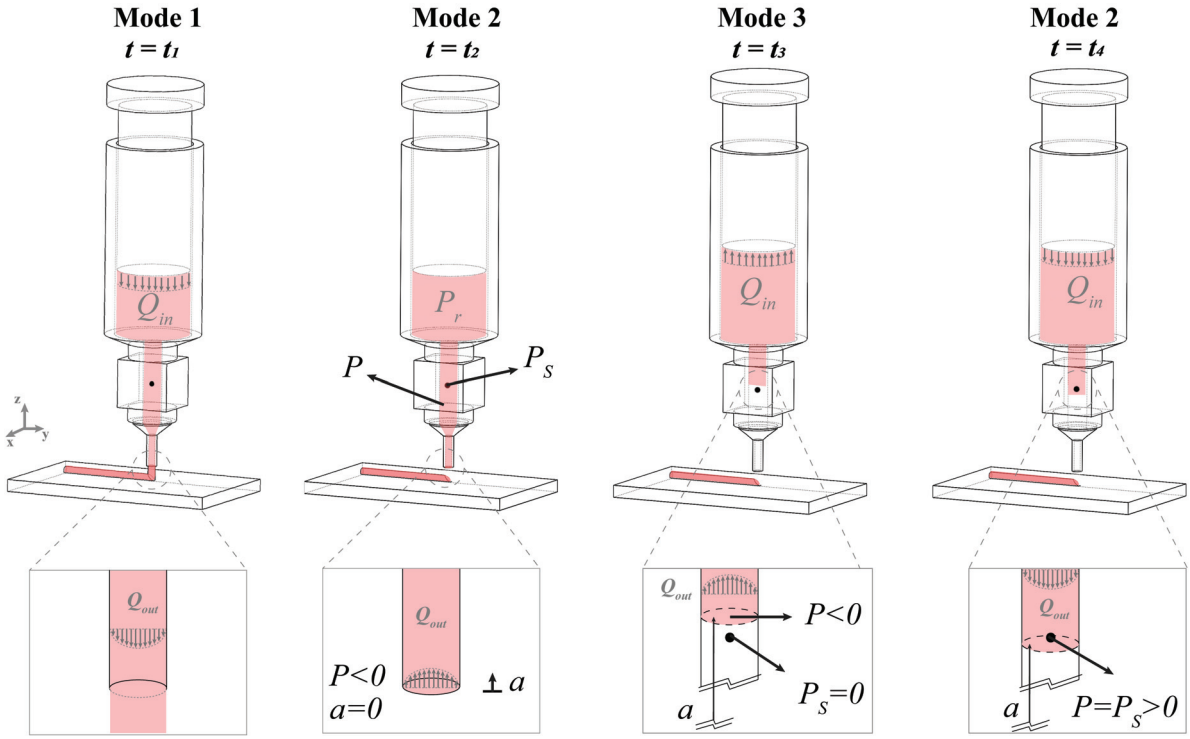

Fig. 1. Sequential modes schematic: At $t = t_1$, ink is being extruded from the nozzle and $P > 0$ (Mode 1). At $t = t_2$, ink extrusion has stopped ($P = 0$ or $P < 0$ and thus the ink leading edge is now greater than or equal to zero ($a \geq 0$, Mode 2). At $t = t_3$ ink loses contact with the pressure sensor ($a > L/2$) and the system enters Mode 3. At $t = t_4$, the ink leading edge is back in contact with the sensor ($0 < a \leqslant L/2$) and thus the system switches back to Mode 2. Note that ($t_4 > t_3 > t_2 > t_1$).

II. Model Development

This section starts with the assumptions in the model development and continues discussing the continuous dynamics, ink leading edge position calculation, switching conditions and finally the hybrid model representation. A state-dependent hybrid model is employed with three discrete modes. In each of these modes continuous dynamics of microextrusion governs the system. Criteria to switch between modes is developed with the ink leading edge position, a, and nozzle pressure, P, as the states.

A. Assumptions

1) Continuous microextrusion:

- **A1.** The ink is Newtonian. Note that this assumption is generally not true, as the inks are often non-Newtonian yield-pseudoplastic materials [3], [7], [18]. Non-Newtonian, hence nonlinear extensions to this work are discussed in Section V.
- **A2.** Microextrusion flow is adiabatic, incompressible, fully developed, and laminar with no slip condition on syringe and nozzle walls.
- **A3.** The change in the input volume (V_{in}) occurs slowly, such that we can assume the reservoir volume is constant on the timescale of the dynamics considered.
- **A4.** The reservoir control volume (V_r), Fig. 2, is large and thus has an appreciable capacitance ($\propto V_r$) and negligible resistance ($\propto 1/{D_r}^4$), where D_r is reservoir diameter. The nozzle control volume is small, inset of Fig. 2, and thus has an appreciable resistance ($\propto 1/D^4$) and negligible capacitance ($\propto V$), where D is nozzle diameter and V is nozzle volume.

2) Discrete switching conditions:

- **A5.** Ink that leaves the nozzle attaches to the substrate and will not retract back into the nozzle.
- **A6.** The pressure sensor and nozzle are combined into one simplified tube, with the sensor acting as a point probe in the middle of the nozzle.

B. Continuous dynamics of microextrusion

The continuous dynamics of microextrusion has been previously developed in the literature [18], [19]. Briefly, the system is divided into two control volumes: 1) the reservoir, which acts like a capacitor, and 2) the nozzle, which acts as a resistor. The circuit analogy and schematic of the system are presented in Fig. 2.

1) Reservoir Control Volume: The Reynolds transport theorem describes the conservation of mass in the reservoir control volume,

$$\frac{dm}{dt} = \frac{d}{dt}\left(\int_{CV} \rho dV\right) + \int_{CS} \rho u_{in} dA_{in} \cdot \hat{n} + \int_{CS} \rho u_{out} dA_{out} \cdot \hat{n} \tag{1}$$

$$\frac{dm}{dt} = \rho\left(Q_{in} - Q_{out}\right) \tag{2}$$

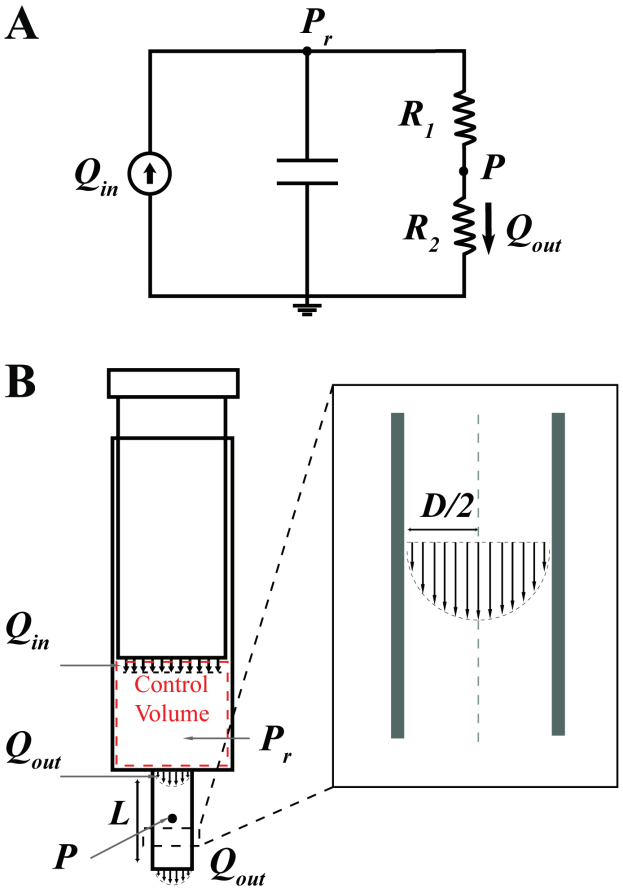

Fig. 2. Continuous flow dynamics. A) Circuit analogy. B) Simplified system demonstrating the reservoir and nozzle control volumes.

$$\left(\frac{dm}{dP_r}\right)\left(\frac{dP_r}{dt}\right) = \rho\left(Q_{in} - Q_{out}\right), \tag{3}$$

where m and ρ are the mass and density of the fluid respectively, dV and dA are the differential volume element and surface area respectively, u_{in} and u_{out} are the inlet and outlet velocity to and from the control volume, $\hat{n}$ is the normal vector to the control surface, P_r is the reservoir pressure, Q_{out} is the output flowrate and Q_{in} is the input flow rate. Fluidic capacitance (C) relates the mass stored (m) to the pressure caused by it [20]. Thus, the transport equation will be simplified as follows,

$$\begin{aligned} \dot{P}_r &= \frac{\rho}{C}(Q_{in} - Q_{out}) \\ C &= \frac{\rho V_r}{\beta}, \end{aligned} \tag{4}$$

where β is the bulk modulus of the fluid, V_r is the reservoir volume ($V_r = V_0 - V_{in}$), V_0 is the total reservoir volume, and V_{in} is the total volume displaced by the plunger.

2) Nozzle Control Volume: Flow in the nozzle control volume is described by the Hagen-Poiseuille model for laminar, fully-developed flow, **A2**, in pipes [20]:

$$R = \frac{\Delta P}{Q} = \frac{128\mu L}{\pi D^4}, \tag{5}$$

where μ is the viscosity, L is the length of the nozzle, D is nozzle diameter, and R is resistance. The flowrate passed through the nozzle is:

$$Q_{out} = \frac{P}{R_2} = \frac{P_r - P}{R_1}. \tag{6}$$

Solving for P_r as a function of P in eq. 6 and plugging it into eq. 4,

$$\dot{P} = \frac{\beta}{V_r R_2}\left(\frac{R_1}{R_2} + 1\right)P + \frac{\beta}{V_r}\left(\frac{R_1}{R_2} + 1\right)Q_{in}. \tag{7}$$

C. Discrete State Model

1) Calculation of ink leading edge position, a: The transition from Mode 1 to Mode 2 is accompanied by a change in the position of the ink leading edge a (Fig. 1) from $a = 0$ (Mode 1) to $a > 0$ (Mode 2 or 3). By assumption **A5**, when ink has left the nozzle, it will never return. Ink is leaving the nozzle when $Q_{out} > 0$ or, equivalently, $P > 0$ and $a = 0$. At the instance of transition from Mode 1 (normal printing) to Mode 2 (leading edge retracted from tip of nozzle), $a = 0$ and $P = 0$. Therefore, the logic in Table I captures the logic for the integration of Q_{out} to compute leading edge position a. The logic uses a $Flag$ to capture the instance when the mode switches from 1 to 2. When in Mode 2, a is simply the negative of the integral of the output flowrate $Q_{out} = \frac{P}{R_2}$ divided by the nozzle cross-sectional area; note that when the integrated flowrate becomes zero again (retraction and then extrusion such that leading edge $a = 0$ again), the mode transitions to Mode 1 and the $Flag$ is reset.

2) Mode switching criteria: The switching conditions are state based and are used to switch between three modes (Fig. 3). Mode 1 is the printing mode, where the ink is in contact with the sensor and a is not being calculated ($a = 0$). $S1$ switches the system to "retracted ink leading edge mode" mode, which is Mode 2 and is when ink is being retracted and a is calculated. $S2$ switches the system back to printing mode, which means there is no need for calculation of a.

$$S1 : a = 0 \quad and \quad P \leq 0 \tag{8}$$

$$S2 : a = 0 \quad and \quad P > 0 \tag{9}$$

$S3$ switches the system form Mode 2 (when the ink is in contact with sensor) to Mode 3 (when the ink loses contact with the sensor) when ink leading edge position passes the sensor location:

$$S3 : a = -\frac{4}{\pi D^2}\int \frac{P}{R_2}dt > \frac{L}{2}, \tag{10}$$

and $S4$ switches the system from Mode 3 back to Mode 2 when the ink gets back in contact with the sensor again:

$$S4 : a = -\frac{4}{\pi D^2}\int \frac{P}{R_2}dt \leqslant \frac{L}{2}. \tag{11}$$

TABLE I

a CALCULATION LOGIC

a **calculation logic pseudo-code**
if $a = 0$ and $P > 0$
Mode 1
$Flag = 0$
$a = 0$
elseif $Flag = 0$ and $P < 0$
Mode 2
$Flag = 1$
elseif $Flag = 1$
Mode 2
$a = -\frac{4}{\pi D^2} \int \frac{P}{R_2} dt$
end

D. Hybrid model

The continuous dynamics and discrete states in Sections II-B and II-C, respectively, are posed as a switched state-space system [21]. Leading edge position a is posed as an augmented state to permit the integration of the pressure signal (Table I).

$$\begin{aligned} \dot{x} &= f(x,u,q) = A_q x + Bu \\ y &= h(x,q) = C_q x \end{aligned} \tag{12}$$

$$x = \begin{bmatrix} P \\ a \end{bmatrix}, \quad A_q = \begin{bmatrix} \frac{\beta}{V_r R_2}\left(\frac{R_1}{R_2}+1\right) & 0 \\ A_{21,q} & 0 \end{bmatrix},$$

$$B = \begin{bmatrix} \frac{\beta}{V_r}\left(\frac{R_1}{R_2}+1\right) \\ 0 \end{bmatrix}, \qquad u = Q_{in},$$

$$y = P_s, \qquad C_q = \begin{bmatrix} c_q & 0 \end{bmatrix},$$

where the state $x \in \mathbb{R}^2$, and $\mathbb{R}^2$ is continuous state space, $u \in \mathbb{R}$, $f : \mathcal{Q} \times \mathbb{R} \times \mathbb{R}^2 \to \mathbb{R}^2$ is the vector field, where $\mathcal{Q}$ is the set of discrete states, and $h : \mathcal{Q} \times \mathbb{R}^2 \to \mathbb{R}$ is the output mapping [22], [23]. To align with hybrid system model notation, mode is denoted by q, of which there are three discrete modes:

$$q \in \mathcal{Q}$$
$$\mathcal{Q} = \{1,2,3\}.$$

The output gain is dependent on the mode and can be described as

$$c_q = \begin{cases} 1 & q = 1 \\ 1 & q = 2 \\ 0 & q = 3 \end{cases}$$

to denote that the pressure, P, is measured by the sensor, P_s, in Modes 1 and 2 (assuming a perfect sensor), but measures the ambient (gauge) pressure in Mode 3. Integrator gain $A_{21,q}$ is also dependent on the mode,

$$A_{21,q} = \begin{cases} 0 & q = 1 \\ -\frac{4}{\pi D^2 R_2} & q = 2 \\ -\frac{4}{\pi D^2 R_2} & q = 3 \end{cases},$$

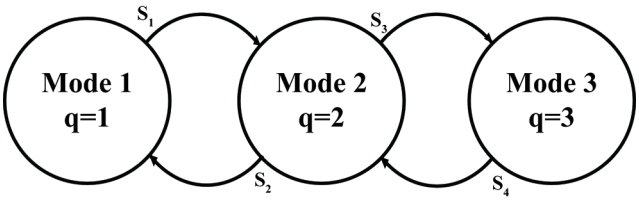

Fig. 3. Schematic of the hybrid model

and prevents the integration of pressure when in mode 1 and enables the integration of pressure with the gain defined in Table I when in modes 2 and 3 resulting in calculation of a.

III. Simulation Methods and Parameters

A. Simulation Method

Model investigation was carried out in a simulation setting. A simulated input flowrate, Q_{in}, is designed to transition through the sequence shown in Fig. 1. Q_{in} represents the piston displacing downward to extrude ink, pausing, then retracting to reverse flow, then displacing down again in two pulses (Fig. 4).

B. Simulation parameters

Simulation parameters are reported in Table II. The assumed parameters are either obtained from the geometric sizes of the μRD system, or from previous experimental work in the literature [18]. A simplified design is employed for simulations where the pressure sensor is in the middle of nozzle, and R_1 and R_2 (Fig. 2) are equal. The assumed ink properties corresponds to a typical ink in food science research with bulk modulus and dynamic viscosity obtained from previous experimental validation from our group [18].

TABLE II

Simulation parameters

Parameter	**Value**
Input amplitude (Q_{in})	2.04×10^{-10} (m^3/s)
Ink bulk modulus (β)	5.67×10^7 (N/m^2)
Ink viscosity (μ)	10^2 $(N.s/m^2)$
Nozzle length (L)	1×10^{-2} (m)
Location of sensor ($L/2$)	0.5×10^{-2} (m)
Nozzle diameter (D)	510 (μm)
Ink volume (V_0)	2×10^{-6} (m^3)
Nozzle Velocity (v)	1 (mm/s)

IV. Results

The flowrate response of the system is shown in Fig. 4. Modes 1 – 3 are color coded to denote active mode. The light gray area corresponds to Mode 1 where normal printing occurs and the ink is in contact with the sensor, dark gray area corresponds to Mode 2 where integration of flowrate is enabled to calculate a and the ink is still in contact with the

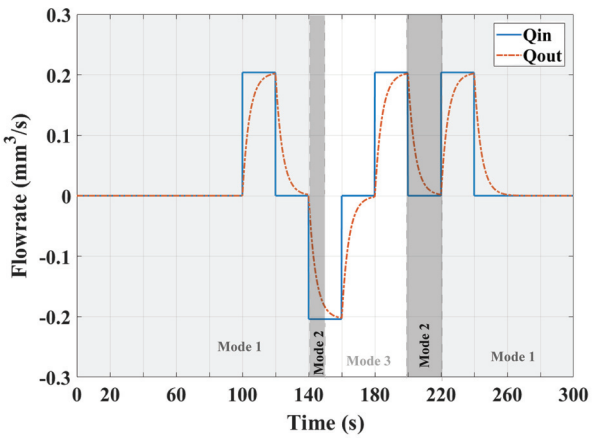

Fig. 4. The output flowrate response (Q_{out}) to the pulse input (Q_{in}) versus time. The solid line corresponds to the input volumetric flowrate and the dashed line corresponds to output flowrate. Different modes are color coded in grayscale.

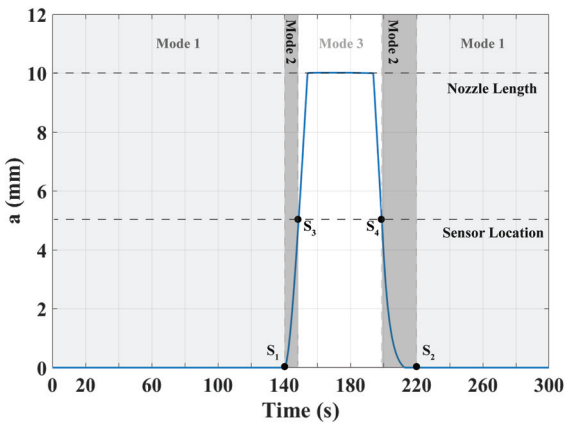

Fig. 5. Ink leading edge position (a) with respect to simulation time. Sensor location and nozzle length at $a = 5mm$ and $a = 10mm$ respectively are marked by horizontal dashed lines.

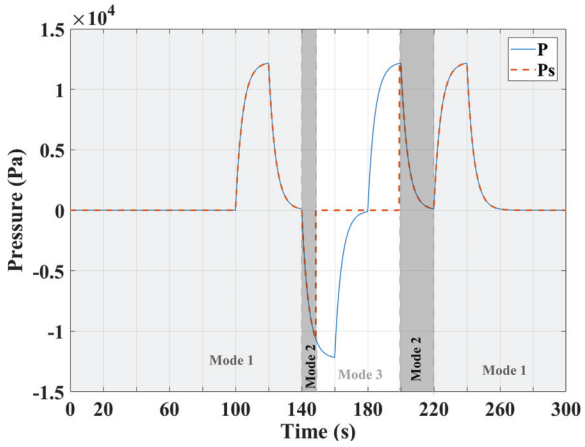

Fig. 6. The actual pressure P and the sensed pressure P_s (Pa) against simulation time. The sensed pressure goes to zero in Mode 3 where the ink loses contact with the sensor.

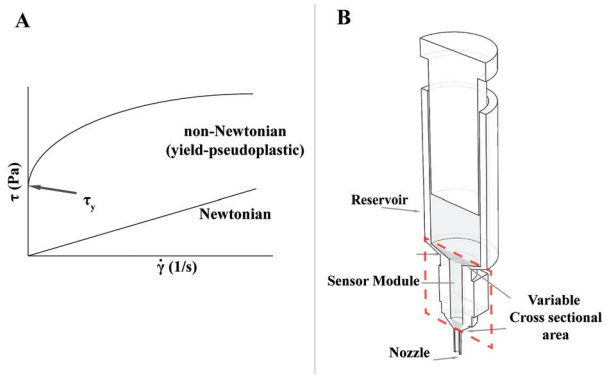

Fig. 7. Ink property and realistic DW AM geometry. A) Shear stress vs shear rate curve demonstrates that non-Newtonian yield-pseudoplastic fluids (YPF) exhibit finite yield stress and a change in viscosity upon applying shear stress. Figure motivated by [24]. B) The realistic geometries of DW AM reservoir, sensor and nozzle is shown. The dashed line demonstrates the region of the control volume that was simplified in our analysis.

sensor, and the white area corresponds to Mode 3 where a is still being calculated but ink is not in contact with the sensor. Fig. 5 shows the calculation of ink leading edge position, a, as a function of time (s). Switching instances are denoted on the plot. $S1$ occurs when $a = 0$ and $P \leq 0$, $S3$ occurs when the calculated ink leading edge position passes the sensor location (dashed horizontal line at a = 5 mm), $S4$ occurs when ink leading edge gets back in contact with the sensor again and $S2$ occurs when $a = 0$ and $P > 0$. The actual pressure P and the output sensed pressure P_s are plotted as a function of time in Fig. 6; as dictated by the switching conditions formalized in Section II-C, $P_s = 0 \neq P$ when the ink leading edge position is beyond the pressure sensor, Mode 3.

V. Discussions and Conclusion

The extrusion-based DW printing model developed here is a switched system that captures continuous printing dynamics and discrete dynamics that transitions between sensor gain and leading edge integration. The simulation results offer a preliminary look into the form of signals expected in an actual system. The output flowrate response follows a typical first order system response to step input. The large time constant is due to the high viscosity of the Newtonian fluid, the fluidic resistance and fluid capacitance (Fig 4). When the ink reaches the sensor location, switching to Mode 3 occurs and, as shown in Fig. 6, this switching occurs right at the time when the loss of pressure signal occurs in Mode 3. Notably, when the ink leading edge reaches the top of the nozzle in Mode 3, the slope of a changes drastically because the diameter of the cross-section area abruptly changes from the small nozzle diameter to large reservoir diameter. The future research avenues are divided into three categories.

1) **Model complexity.** This preliminary model will be modified to include a more realistic continuous and discrete systems. Current, validated DW AM models use non-Newtonian fluid mechanics (Fig. 7 A), which are more realistic for the inks used in DW AM. Here,

the fluid was considered to be Newtonian due their relative simplicity compared to other types as a preliminary study of the switching criteria. The transition to non-Newtonian fluid models will result in a nonlinear continuous fluid mechanics model. Moreover, the reservoir, sensor channel, and nozzle geometry was simplified to be two channels with uniform cross-section. Actual DW reservoirs, nozzles, and transitions between them are of variable cross-sectional area (Fig. 7 B), increasing the complexity of the computation of a in Table I.

2) **Physical implementation.** There are considerable, interesting challenges in physical implementation and subsequent model validation. Beyond standard validation issues such as pressure sensor noise and bias, which challenges the demarcation of transitions between modes, the leading edge a is not sensed. State estimators will be required to estimate a from available input measurements Q_{in} and output measurements P_s. This estimator, likewise, will have to have a switched architecture as P_s transitions from sensed to not sensed (Mode 2 to Mode 3).
3) **Control analysis, design, and application.** The hybrid model developed here paves the way for hybrid control design and accompanying stability analyses. While hybrid models provide a good basis for process control, complexities arises in the stability analysis of switched systems which will be further studied in future works. The integrated system will be applied to biomedical applications, in which the precise control over flowrate is crucial.

ACKNOWLEDGMENT

The authors would like to acknowledge Andrej Simeunovic at OSU, and Drs. Amir Sheikhi and Ali Khademhosseini at UCLA for their thoughtful discussions and advice during the production of this work.

REFERENCES

[1] T. J. Horn and O. L. A. Harrysson, "Overview of current additive manufacturing technologies and selected applications," *Science Progress*, vol. 95, no. 3, pp. 255–282, 2012.
[2] J. E. Smay, J. Cesarano, and J. A. Lewis, "Colloidal Inks for Directed Assembly of 3-D Periodic Structures," *Langmuir*, vol. 18, no. 14, pp. 5429–5437, July 2002.
[3] D. J. Hoelzle, S. R. Svientek, A. G. Alleyne, and A. J. Wagoner Johnson, "Design and Manufacture of Combinatorial Calcium Phosphate Bone Scaffolds," *Journal of Biomechanical Engineering*, vol. 133, no. 10, pp. 101 001–101 001–8, Oct. 2011.
[4] S. Michna, W. Wu, and J. A. Lewis, "Concentrated hydroxyapatite inks for direct-write assembly of 3-D periodic scaffolds," *Biomaterials*, vol. 26, no. 28, pp. 5632–5639, Oct. 2005.
[5] L. E. Bertassoni, J. C. Cardoso, V. Manoharan, A. L. Cristino, N. S. Bhise, W. A. Araujo, P. Zorlutuna, N. E. Vrana, A. M. Ghaemmaghami, M. R. Dokmeci, and A. Khademhosseini, "Direct-write bioprinting of cell-laden methacrylated gelatin hydrogels," *Biofabrication*, vol. 6, no. 2, p. 024105, 2014.
[6] Y. Xie, L. E. Rustom, A. M. McDermott, J. D. Boerckel, A. J. W. Johnson, A. G. Alleyne, and D. J. Hoelzle, "Net shape fabrication of calcium phosphate scaffolds with multiple material domains," *Biofabrication*, vol. 8, no. 1, p. 015005, Jan. 2016.
[7] J. A. Lewis, "Direct Ink Writing of 3d Functional Materials," *Advanced Functional Materials*, vol. 16, no. 17, pp. 2193–2204, Nov. 2006.
[8] X. Zhao, R. G. Landers, and M. C. Leu, "Adaptive Extrusion Force Control of Freeze-Form Extrusion Fabrication Processes," *Journal of Manufacturing Science and Engineering*, vol. 132, no. 6, pp. 064 504–064 504–9, Dec. 2010.
[9] M. Li, L. Tang, R. G. Landers, and M. C. Leu, "Extrusion Process Modeling for Aqueous-Based Ceramic PastesPart 1: Constitutive Model," *Journal of Manufacturing Science and Engineering*, vol. 135, no. 5, pp. 051 008–051 008–7, Sept. 2013.
[10] D. J. Hoelzle, A. G. Alleyne, and A. J. W. Johnson, "Basis Task Approach to Iterative Learning Control With Applications to Micro-Robotic Deposition," *IEEE Transactions on Control Systems Technology*, vol. 19, no. 5, pp. 1138–1148, Sept. 2011.
[11] R. P. Chhabra and J. F. Richardson, *Non-Newtonian Flow and Applied Rheology: Engineering Applications*. Butterworth-Heinemann, Apr. 2011.
[12] C. Tomlin, G. J. Pappas, and S. Sastry, "Conflict resolution for air traffic management: a study in multiagent hybrid systems," *IEEE Transactions on Automatic Control*, vol. 43, no. 4, pp. 509–521, Apr. 1998.
[13] R. W. Brockett, "Hybrid Models for Motion Control Systems," in *Essays on Control: Perspectives in the Theory and its Applications*, ser. Progress in Systems and Control Theory. Boston, MA: Birkhuser Boston, 1993, pp. 29–53.
[14] J. Poon, P. Jain, I. C. Konstantakopoulos, C. Spanos, S. K. Panda, and S. R. Sanders, "Model-Based Fault Detection and Identification for Switching Power Converters," *IEEE Transactions on Power Electronics*, vol. 32, no. 2, pp. 1419–1430, Feb. 2017.
[15] M. Egerstedt and X. Hu, "A hybrid control approach to action coordination for mobile robots," *Automatica*, vol. 38, no. 1, pp. 125–130, Jan. 2002.
[16] L. Chaimowicz, M. F. M. Campos, and V. Kumar, "Hybrid systems modeling of cooperative robots," in *2003 IEEE International Conference on Robotics and Automation*, vol. 3, 2003, pp. 4086–4091 vol.3.
[17] M. Diagne, P. M. Sammons, D. Hoelzle, and K. L. Barton, "Hybrid Continuous-Discrete Repetitive Process Modeling of Meniscus Dynamics in Electrohydrodynamic Jet Printing," *IFAC-PapersOnLine*, vol. 50, no. 1, pp. 13 414–13 419, July 2017.
[18] A. Simeunovic and D. J. Hoelzle, "Nonlinear and linearized gray box models of direct-write printing dynamics," in *Proceedings of the 29th Anuual International Solid Freeform Fabrication Symposium*, 2018, pp. 1953–1975.
[19] D. J. Hoelzle, A. G. Alleyne, and A. J. W. Johnson, "Iterative Learning Control for robotic deposition using machine vision," in *2008 American Control Conference*, June 2008, pp. 4541–4547.
[20] W. J. Palm, *System dynamics*. McGraw-Hill, 2014.
[21] D. Liberzon, *Switching in Systems and Control*, ser. Systems & Control: Foundations & Applications. Birkhuser Basel, 2003.
[22] J. P. Hespanha, "Modeling and analysis of networked control systems using stochastic hybrid systems," *Annual Reviews in Control*, vol. 38, no. 2, pp. 155–170, Jan. 2014.
[23] M. S. Branicky, "Introduction to Hybrid Systems," in *Handbook of Networked and Embedded Control Systems*, ser. Control Engineering, D. Hristu-Varsakelis and W. S. Levine, Eds. Boston, MA: Birkhuser Boston, 2005, pp. 91–116.
[24] J. A. Lewis, "Colloidal Processing of Ceramics," *Journal of the American Ceramic Society*, vol. 83, no. 10, pp. 2341–2359, 2000.